

Supplementary Material for

A Combined Experimental and Modeling Study on Isopropyl Nitrate Pyrolysis

Nicolas Vin^{1,#}, Hans-Heinrich Carstensen^{2,3}, Olivier Herbinet^{1,*}, Jérémy Bourgalais¹, María Ujué Alzueta⁴, Frédérique Battin-Leclerc¹

¹Université de Lorraine, CNRS, LRGP, Nancy, 54000, France.

²Fundación Agencia Aragonesa para la Investigación y el Desarrollo (ARAID), Zaragoza, 50018, Spain

³Escuela de Ingeniería y Arquitectura, Universidad de Zaragoza, Zaragoza, 50018, Spain

⁴Aragón Institute of Engineering Research (I3A), Zaragoza, 50018, Spain

Content

1. Temperature profiles	2
2. Elemental balances	3
3. List of names and structures of nitrogen containing species	4
4. Geometries, frequencies, rotational constants and NASA polynomials for iPN and its radical C ₂ JCONO ₂	6
5. Experimental results and model comparisons.....	10
6. Pressure-dependent rate coefficients for iPN decomposition	16
7. Ab initio energies related to iPN and CH ₃ NO ₂	17
8. PES of C ₂ JCONO ₂	18
9. Pressure-dependent rate expressions for unimolecular decomposition of the iPN radical CH ₃ C(H)(ONO ₂)CH ₂ , labelled C ₂ JCONO ₂	19
10. High-pressure limit rate coefficients for CH ₃ NO ₂ → CH ₃ +NO ₂	21
11. Brief review of the High-pressure limit rate coefficients for the reactions CH ₃ +NO ₂ → CH ₃ O+NO and CH ₃ +NO ₂ → CH ₃ NO ₂	22
12. References	24

* Corresponding author: olivier.herbinet@univ-lorraine.fr

Present adress: #N.V.: IFP Energies Nouvelles, Solaize, 69360, France

1. Temperature profiles

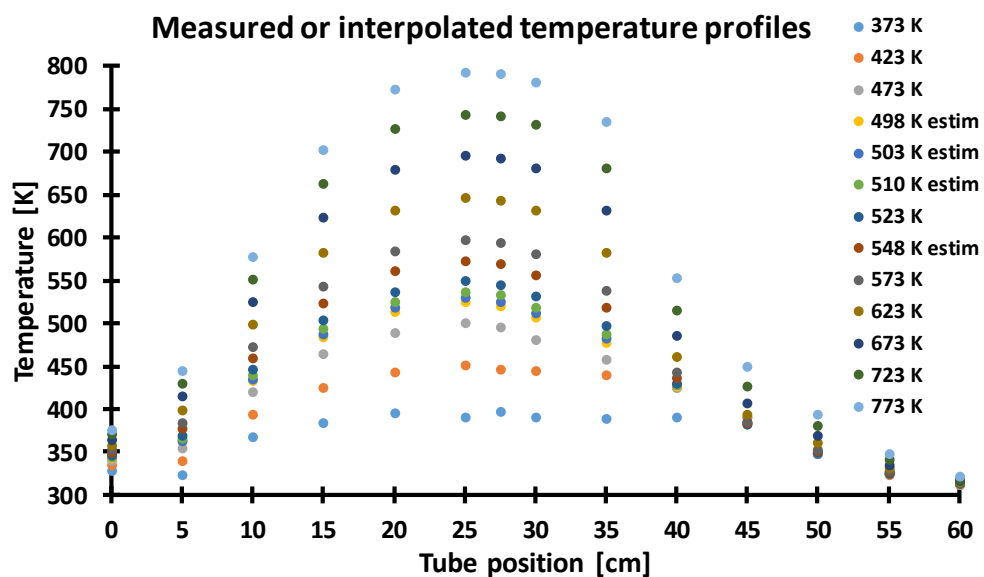


Figure S1: Actual temperature profiles for various set temperatures as a function of distance. The reactive (hot zone) is approximately 30 cm.

The temperature profiles as shown in Figure S1 are used as input for the Chemkin simulations.

Table S1: initial flow velocities used in the Chemkin simulations for approximately 2 s residence time in the hot zone.

Set temperature [K]	373	423	473	498	503	510	523	548	573	623	673	723	773
Flow velocity [cm/s] at x = 0 cm	13.2	11.8	10.8	10.3	10.2	10.1	9.9	9.6	9.2	8.6	8.1	7.7	7.3

2. Elemental balances

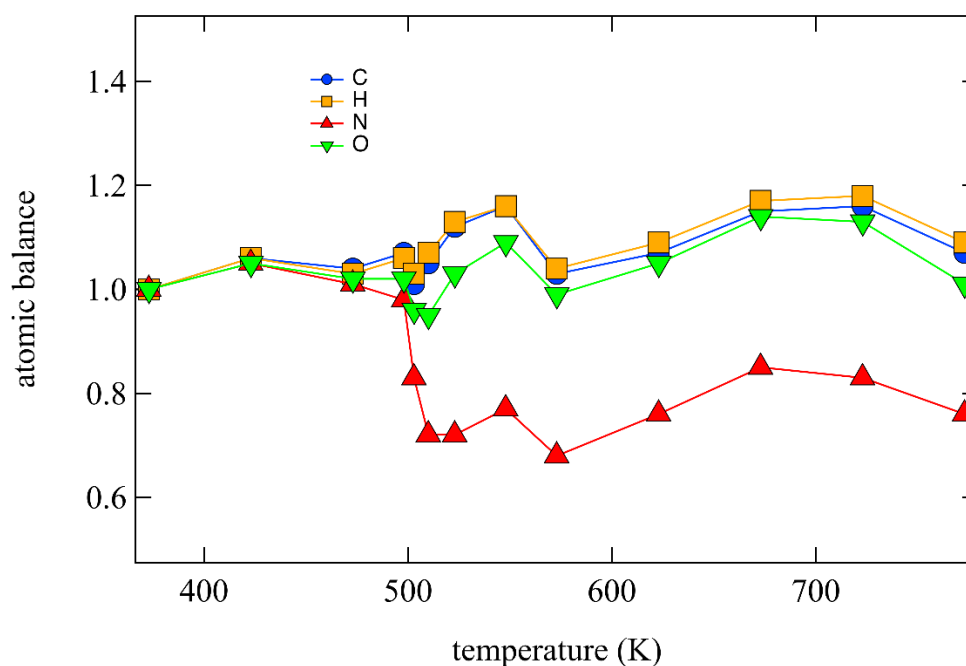
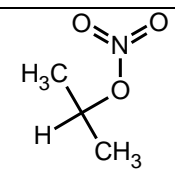
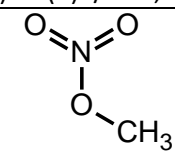
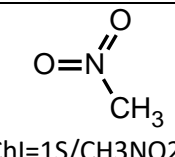
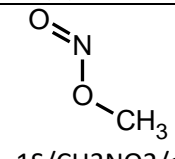
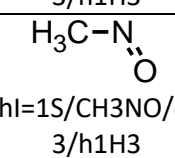
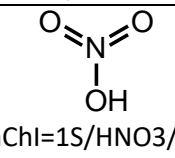
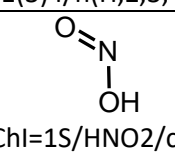
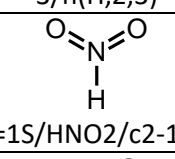
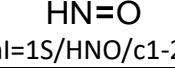
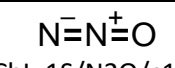


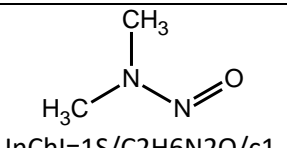
Figure S2: Elemental balances in C (blue dots), H (orange squares), N (red triangles), and O (down green triangles) during iPN pyrolysis for an inlet mole fraction of 0.01 and a residence time of 2s at atmospheric pressure.

The balances are calculated with the quantified species. Some products such as molecular nitrogen have been detected but not quantified. The balances for hydrogen and carbon run almost on top of each other and are constantly around or above 100% suggesting that the major carbon and hydrogen containing species have been detected, but also that the quantification error is about 20 % and not 10% are normally estimated. In contrast to hydrogen and carbon, a large amount of nitrogen is missing. A possible explanation is that substantial quantities of molecular nitrogen (N_2) are produced. The rather high fluctuations in the balances serves as an indication that these experiments were difficult to conduct in a controlled manner due to the high reactivity of iPN.

3. List of names and structures of nitrogen containing species

Table S2: Names (IUPAC names are in parentheses, if different) of nitrogen species used in the text, formulas and structures.

Name	Formula		Structure
iPN isopropyl nitrate (propane-2-yl-nitrate)	$C_3H_7O_3N$	$(CH_3)_2C(H)ONO_2$	 <chem>InChI=1S/C3H7NO3/c1-3(2)7-4(5)6/h3H,1-2H3</chem>
Methyl nitrate	CH_3O_3N	CH_3ONO_2	 <chem>InChI=1S/CH3NO3/c1-5-2(3)4/h1H3</chem>
Nitromethane	CH_3O_2N	CH_3NO_2	 <chem>InChI=1S/CH3NO2/c1-2(3)4/h1H3</chem>
Methyl nitrite	CH_3O_2N	CH_3ONO	 <chem>InChI=1S/CH3NO2/c1-4-2-3/h1H3</chem>
Nitrosomethane	CH_3ON	CH_3NO	 <chem>InChI=1S/CH3NO/c1-2-3/h1H3</chem>
Nitric acid	HO_3N	$HONO_2$	 <chem>InChI=1S/HNO3/c2-1(3)4/h(H,2,3,4)</chem>
Nitrous acid	HO_2N	$HONO$	 <chem>InChI=1S/HNO2/c2-1-3/h(H,2,3)</chem>
Nitryl hydride	HO_2N	HNO_2	 <chem>InChI=1S/HNO2/c2-1-3/h1H</chem>
Nitrosyl hydride	HON	HNO	 <chem>InChI=1S/HNO/c1-2/h1H</chem>
Nitrous oxide (Dinitrogen oxide)	ON_2	N_2O	 <chem>InChI=1S/N2O/c1-2-3</chem>

Nitric oxide (Nitrogen monoxide)	ON	NO	$\text{N}=\dot{\text{O}}$ InChI=1S/NO/c1-2
Nitrogen dioxide	O ₂ N	NO ₂	$\text{O}=\text{N}-\dot{\text{O}}$ InChI=1S/NO2/c2-1-3
Hydrogen cyanide Hydrocyanic acid (Formonitrile)	HCN	HCN	$\text{H}-\text{C}\equiv\text{N}$ InChI=1S/CHN/c1-2/h1H
Dimethylnitrosoamine (<i>N,N</i> -Dimethylnitrous amide)	C ₂ H ₆ ON ₂	(CH ₃) ₂ NNO	 InChI=1S/C2H6N2O/c1-4(2)3-5/h1-2H3

4. Geometries, frequencies, rotational constants and NASA polynomials for iPN and its radical C₂JCONO₂

Table S3: Ab initio results (G4 level) for iPN and C₂JCONO₂ and the transition states and products of Figure 1 of the main text

Species	Cartesian coordinates [Å]	Frequencies [cm ⁻¹] and rotational constants [GHz]	
iPN	6 0.047186 0.023306 -0.030010	90.0854 106.1961 206.9888	
	6 -0.056834 -0.047995 1.488193	214.7314 261.3817 322.3204	
	6 1.482004 0.079685 -0.540908	405.8520 453.5052 568.5440	
	8 -0.607747 -1.198310 -0.488712	711.5487 782.6596 859.9780	
	1 -0.527870 0.868923 -0.413791	892.0928 928.9540 940.9300	
	1 -1.100548 -0.107914 1.805603	952.2768 1135.6135 1162.1895	
	1 0.475921 -0.921465 1.875125	1202.1936 1322.8719 1358.8656	
	1 0.389943 0.849152 1.925862	1393.8716 1402.6688 1418.8828	
	1 1.509654 0.111137 -1.631745	1480.2485 1485.1949 1495.6794	
	1 1.972430 0.981949 -0.162742	1511.5229 1738.2100 3045.4229	
	1 2.046822 -0.790830 -0.193869	3049.7148 3089.0515 3115.8103	
	7 -1.080717 -1.171230 -1.812793	3126.6223 3131.1882 3139.0071	
	8 -1.575768 -2.213387 -2.146984		
	8 -0.952624 -0.146237 -2.443562	1.536 1.786 5.137	
	iPN	H 7C 3N 1O 3g 300.000 2500.0001000.000	
1	0.72475343E+01 0.39542917E-01-0.22450678E-04 0.61825420E-08-0.67129039E-12		
2	-0.27905264E+05-0.90460577E+01 0.15104003E+01 0.51236853E-01-0.20787264E-04		
3	-0.10218295E-07 0.81117014E-11-0.26225957E+05 0.21330215E+02		
4			
C ₂ JCONO ₂	1 -0.084070 -0.245376 0.012601	81.9435 95.2294 131.9317	
	6 -0.027562 0.025507 1.058321	209.8893 243.7192 318.8012	
	6 1.258263 -0.046912 1.796799	384.6233 449.3544 527.5184	
	8 1.962915 1.258960 1.761185	628.8361 709.7643 782.9380	
	7 2.571204 1.566930 0.534773	859.7924 876.4775 906.4277	
	8 3.091877 2.650131 0.534119	928.5867 1044.0103 1159.4438	
	8 2.515219 0.743181 -0.350803	1192.3081 1313.8568 1361.6346	
	1 1.930343 -0.775220 1.339397	1374.3104 1407.7112 1459.0447	
	1 -0.895494 0.470291 1.532681	1484.7938 1496.1592 1733.6698	
	6 1.096801 -0.312617 3.288974	3049.5513 3097.2966 3128.1670	
	1 2.067691 -0.309563 3.790131	3132.4458 3157.8022 3275.5906	
	1 0.461648 0.448034 3.751670		
	1 0.627889 -1.289480 3.433913	1.558 1.837 5.360	
	C ₂ JCONO ₂	H 6C 3N 1O 3g 300.000 2500.0001000.000	
	1	0.10081143E+02 0.31013502E-01-0.17238111E-04 0.46821427E-08-0.50382918E-12	
2	-0.37229949E+04-0.20486778E+02 0.35859108E+01 0.48113476E-01-0.27838816E-04		
3	-0.17356638E-09 0.43496933E-11-0.20009596E+04 0.12986263E+02		
4			
C ₂ COJ	6 0.033006 -0.016611 -0.019616	190.8015 230.7197 349.8668	
	6 -0.008181 -0.015496 1.518471	387.8979 445.4099 804.4343	
	8 1.232387 -0.132888 2.082448	886.5240 908.8721 982.9725	
	6 -0.825907 1.145131 2.111501	1044.0154 1077.3102 1157.8245	
	1 -0.494203 -0.966351 1.840936	1199.3871 1250.5496 1380.3365	
	1 0.611435 -0.869920 -0.381492	1404.6379 1477.9977 1483.7972	

	1	-0.975845	-0.065503	-0.440581	1493.0006	1502.2256	2833.5247
	1	0.508586	0.900836	-0.381085	3035.8372	3042.2837	3108.0366
	1	-1.857395	1.126877	1.746706	3114.0127	3128.0542	3129.6299
	1	-0.832985	1.083717	3.202305			
	1	-0.379596	2.102180	1.822698	4.833	8.029	9.207
NO2	7	0.076618	0.000000	0.036881	756.0921	1399.2198	1722.9944
	8	0.035604	0.000000	1.231854			
	8	0.960240	0.000000	-0.768638	12.344	13.011	240.875
C2C=O	6	-0.000603	-0.000040	0.000825	61.5988	145.5802	373.7167
	1	-0.011793	0.005274	1.096757	490.1220	527.8893	781.3317
	1	1.052259	-0.005179	-0.303607	880.2317	880.9075	1082.2544
	1	-0.487809	0.899775	-0.376091	1117.9110	1229.8337	1381.6309
	6	-0.710788	-1.234774	-0.529580	1382.3347	1458.7529	1465.6299
	6	-0.144291	-2.574712	-0.089228	1468.5431	1488.2072	1820.9263
	1	0.903724	-2.665503	-0.396879	3031.5208	3038.2954	3090.6853
	1	-0.160022	-2.654990	1.003716	3097.9214	3152.0703	3153.2605
	1	-0.727141	-3.386358	-0.525826			
	8	-1.670832	-1.155660	-1.259592	4.896	8.490	10.122
HONO	7	-0.156640	0.000000	-0.052490	598.3454	642.3812	861.5233
	8	0.140684	0.000000	1.080528	1318.3408	1785.8701	3758.4612
	8	1.000905	0.000000	-0.878380			
	1	0.620453	0.000000	-1.769514	11.146	12.649	93.771
CC=C	6	0.047038	-0.008755	0.024963	212.2931	420.6988	591.5971
	1	-0.519810	-0.323411	0.910094	927.5674	943.9329	944.3211
	1	1.081581	0.143862	0.356944	1036.4019	1071.4468	1190.1816
	1	0.038367	-0.831858	-0.695451	1329.0647	1406.1025	1451.0846
	6	-0.523186	1.246456	-0.565548	1480.0990	1494.1188	1722.0784
	6	-0.987364	1.370900	-1.804887	3019.4277	3067.1130	3104.8306
	1	-0.547134	2.111572	0.096462	3133.3823	3142.9873	3222.7300
	1	-1.388845	2.308065	-2.175556			
	1	-0.984247	0.536553	-2.501256	8.136	9.276	47.013
HONO2	7	-0.130936	0.000000	0.073952	511.5829	588.1259	662.4968
	8	-0.252012	0.000000	1.264192	788.7817	923.6903	1338.7280
	8	1.204475	0.000000	-0.363780	1369.1871	1793.8695	3723.1980
	1	1.107778	0.000000	-1.331093			
	8	-0.967604	0.000000	-0.801222	6.282	12.149	13.011
TS to CC=C+HONO2	6	0.003651	-0.015007	-0.001444	-844.5381	37.6650	73.3421
	6	0.013715	-0.022820	1.482288	176.3125	221.5086	316.8825
	6	1.184826	-0.000818	2.256505	364.2115	441.9586	528.1593
	8	-0.789090	2.031031	1.597858	589.5739	711.3638	775.8819
	7	-0.176990	2.903122	2.288929	821.5281	875.6049	945.5195
	8	0.983979	2.602760	2.752143	968.5398	1002.5292	1052.1830
	1	-0.874225	0.497972	-0.396588	1088.0365	1205.8613	1277.0385
	1	0.913942	0.428768	-0.411134	1348.4294	1386.4105	1390.3082
	1	-0.039391	-1.062826	-0.335550	1436.9441	1463.4171	1489.0999
	1	-0.930852	-0.243789	1.968678	1529.6025	1595.3270	1629.6987
	1	1.165368	1.226056	2.510035	3013.7036	3097.9404	3101.0530
	1	2.125506	-0.146677	1.725591	3151.8606	3178.9473	3202.8127
	1	1.135825	-0.463641	3.240836			
	8	-0.659704	3.988849	2.508758	1.342	1.640	5.072

TS to C2C=O+HONO	6	0.070990	-0.384653	0.046875	-1321.1641	100.4569	154.0740
	6	-0.041373	-0.012313	1.533209	163.0649	179.4068	241.0259
	6	1.378588	-0.011886	-0.668447	328.9661	379.7013	401.1079
	8	-0.526679	-1.460884	-0.338803	487.1156	536.2802	586.7536
	1	-0.777158	0.421361	-0.499962	801.7503	832.0854	917.1511
	1	-1.048392	-0.224945	1.899656	965.3649	1064.4103	1134.2802
	1	0.667199	-0.612650	2.116099	1152.0988	1182.9199	1329.8730
	1	0.190273	1.042693	1.704100	1381.6808	1392.3243	1444.3470
	1	1.296837	-0.223516	-1.737147	1471.3469	1479.8751	1488.0818
	1	1.630011	1.042945	-0.526963	1502.9874	1637.4338	1790.5071
	1	2.201805	-0.612766	-0.264102	3030.1104	3034.4734	3099.8879
	7	-2.095951	-0.667807	-1.350599	3103.4983	3131.2544	3133.2295
	8	-2.999515	-1.180793	-1.933331			
	8	-1.899553	0.550360	-1.223702	1.466	1.517	4.819
NO3	7	0.000005	0.000000	0.000002	186.3314	186.5920	810.4384
	8	-0.225304	0.000000	1.212302	1141.7720	1141.7939	1143.2104
	8	1.162550	0.000000	-0.411028			
	8	-0.937212	0.000000	-0.801291	6.927	13.854	13.854
Ccy(CCO)	6	-0.014011	-0.055335	0.003294	208.0793	363.6747	406.0796
	8	-0.090520	0.119886	1.419097	780.2311	854.3609	904.1112
	6	1.203031	-0.006060	0.822970	979.6546	1041.1487	1132.0608
	6	2.093503	1.207909	0.873211	1157.9005	1164.1545	1186.6899
	1	1.693668	-0.955986	1.043749	1298.6926	1403.3386	1439.7327
	1	-0.293728	0.814578	-0.590432	1483.4558	1497.3125	1532.8972
	1	2.922367	1.108008	0.163984	3035.2012	3077.9905	3088.8003
	1	1.528480	2.111062	0.626656	3100.2795	3121.7605	3163.7795
	1	2.520472	1.333616	1.873665			
	1	-0.382400	-1.009123	-0.372620	5.926	6.640	18.216
Ccy(CON(OJ)OC)	7	0.024675	-0.119288	0.086018	64.4436	194.5445	244.3733
	8	0.177742	0.393614	1.158021	331.5946	374.6574	435.1152
	8	1.217758	-0.207173	-0.806074	575.7807	613.8443	661.0418
	6	0.750146	-0.158598	-2.154413	689.5977	813.1717	842.8976
	6	-0.786180	-0.208668	-2.013767	953.0466	968.3797	1030.5507
	8	-1.034714	0.416351	-0.769169	1082.8358	1125.5717	1162.1665
	1	-1.295597	0.378613	-2.779724	1248.8872	1318.5804	1366.5355
	6	1.259811	1.113980	-2.820968	1381.4696	1409.6461	1484.6342
	1	0.990771	1.121601	-3.882661	1496.0673	1501.0239	1577.7616
	1	0.825691	1.994812	-2.339180	3031.2954	3039.6460	3051.1082
	1	2.347915	1.175913	-2.740960	3114.3914	3124.8418	3130.0525
	1	1.115472	-1.050384	-2.675451			
	1	-1.164196	-1.238048	-2.017818	1.919	2.347	5.054
	TS to CC=C+NO3	6	-0.019161	0.010776	0.005746	-181.7872	72.3968
6		-0.009323	0.091743	1.496962	133.2493	164.1617	213.1008
6		1.130330	0.056734	2.257604	253.4611	422.1740	528.3700
8		-0.251551	2.208107	1.698477	614.5212	690.9948	805.2186
7		-0.911601	2.583814	2.792934	911.4778	915.6688	947.3567
8		-1.136602	1.769570	3.670490	951.7893	984.2250	1063.2853
8		-1.230851	3.759483	2.782301	1198.6980	1292.9375	1316.9849
1		-0.958568	-0.042953	2.003986	1395.9125	1431.7632	1472.9500
1		-0.733712	0.725965	-0.410448	1489.2834	1561.2346	1626.1077
1		0.967693	0.204184	-0.421335	3033.2893	3099.4460	3132.2549

	1	-0.342341	-0.990463	-0.305851	3156.9080	3199.5847	3262.6157
	1	1.073804	0.057219	3.339120			
	1	2.113214	0.098713	1.799176	1.353	1.550	5.311
TS to Ccy(CCO)+NO2	8	0.052810	-0.027793	0.084564	-707.7162	63.9958	104.2592
	6	0.065758	0.001770	2.023229	152.7369	231.9499	270.7526
	6	1.131213	-0.002686	1.001600	324.5921	393.4706	435.8866
	1	1.711696	-0.932458	0.971411	460.1827	550.6585	726.0758
	6	2.021980	1.224091	0.913367	771.9595	853.7033	922.8477
	1	1.418270	2.136074	0.941737	929.7002	1094.5273	1160.9886
	1	2.726487	1.241249	1.751215	1194.5658	1292.4991	1362.9366
	1	2.596370	1.211723	-0.015872	1394.4093	1416.0946	1461.8173
	7	0.566839	-0.356764	-1.614616	1487.0610	1499.6619	1773.0829
	8	-0.338377	-0.272400	-2.381564	3038.2876	3042.6960	3115.3481
	8	1.709170	-0.697538	-1.737752	3131.3257	3172.4172	3291.6785
	1	-0.383328	0.938952	2.326715			
	1	-0.389271	-0.925287	2.344356	1.446	1.735	4.888
TS to Ccy(CON(OJ)OC)	6	0.127809	0.075624	0.015600	-729.4960	101.7768	177.5622
	6	0.133989	0.111349	1.503746	245.4450	312.2793	443.4334
	6	1.442787	-0.303432	2.167109	483.3104	545.5311	584.3646
	8	-0.087972	1.503281	1.936379	655.6867	691.3829	820.1042
	7	-0.749097	2.210643	0.925512	856.2704	863.7142	916.1948
	8	-0.458657	3.386986	0.795890	954.9078	1048.6605	1141.9154
	8	-1.265952	1.435535	0.068615	1157.2957	1185.9297	1349.3933
	1	0.929547	0.572300	-0.521598	1370.8811	1407.9489	1463.5447
	1	1.628296	-1.366591	1.992630	1485.8438	1494.7466	1579.7024
	1	2.279287	0.273467	1.764324	3048.4785	3058.2732	3124.4417
	1	1.389733	-0.134943	3.246110	3132.0840	3155.7004	3271.6191
	1	-0.701622	-0.480962	1.890558			
	1	-0.388673	-0.723985	-0.497576	1.737	2.169	5.368

5. Experimental results and model comparisons

Table S4: Mole fraction data as function of temperature. Additional species such as molecular nitrogen were detected but not quantified.

Species / detector		373 K	423 K	473 K	498 K	503 K	510 K	523 K	548 K	573 K	623 K	673 K	723 K	773 K
iPN	GC	1.0E-2	1.1E-2	9.6E-3	7.7E-3	5.0E-3	1.3E-3	1.9E-4	-	-	-	-	-	-
	FTIR	9.9E-3	9.6E-3	9.0E-3	4.9E-3	2.4E-3	3.2E-4	3.7E-5	-	-	-	-	-	-
CH2O	GC	-	-	2.9E-4	1.1E-3	1.5E-3	2.8E-3	3.9E-3	5.9E-3	8.2E-3	8.9E-3	9.6E-3	1.0E-2	9.9E-3
	FTIR	-	-	3.5E-4	-	2.2E-3	4.2E-3	6.0E-3	7.1E-3	7.4E-3	7.9E-3	8.6E-3	8.0E-3	7.1E-3
CH3CHO	GC	-	-	7.0E-4	3.3E-3	4.1E-3	7.4E-3	8.3E-3	8.5E-3	7.1E-3	7.1E-3	7.1E-3	7.2E-3	5.8E-3
CH3OH	FTIR	-	-	-	-	1.1E-3	1.7E-3	2.2E-3	2.8E-3	3.6E-3	4.1E-3	4.4E-3	4.3E-3	4.1E-3
CO	FTIR	-	-	-	-	2.9E-4	4.8E-4	8.9E-4	1.3E-3	1.6E-3	2.0E-3	2.5E-3	3.0E-3	3.8E-3
NO	FTIR	-	-	9.6E-5	-	3.8E-4	6.5E-4	1.2E-3	2.2E-3	3.5E-3	4.9E-3	5.7E-3	5.6E-3	6.1E-3
CH4	GC	-	-	-	3.5E-5	4.3E-5	8.0E-5	1.0E-4	1.4E-4	2.8E-4	6.1E-4	9.3E-4	1.6E-3	2.7E-3
	FTIR	-	-	-	-	1.2E-4	-	1.2E-4	3.5E-4	2.4E-4	7.3E-4	1.2E-3	1.7E-3	2.9E-3
CH3ONO	GC	-	-	1.1E-4	7.8E-4	1.2E-3	2.3E-3	2.6E-3	2.1E-3	3.1E-4	3.7E-5	2.2E-5	-	-
CH3NO2	GC	-	-	2.0E-4	8.8E-4	1.2E-3	2.1E-3	2.5E-3	2.6E-3	2.3E-3	2.4E-3	2.5E-3	2.5E-3	1.3E-3
HC(*O)NH2	GC	-	-	3.3E-5	3.0E-4	3.9E-4	7.0E-4	7.5E-4	8.9E-4	6.1E-4	2.0E-4	1.2E-4	1.2E0 5	-
CO2	GC	-	-	-	1.5E-4	1.4E-4	2.7E-4	2.6E-4	2.9E-4	2.4E-4	2.8E-4	2.9E-4	3.5E-4	3.1E-4
	FTIR	-	-	-	-	-	4.9E-6	1.8E-4	2.3E-4	2.1E-4	1.8E-4	2.4E-4	2.4E-4	2.5E-4
C2COH	GC	-	-	1.1E-5	1.0E-4	1.7E-4	2.9E-4	2.4E-4	6.5E-5	5.1E-5	5.3E-5	5.9E-5	6.1E-5	4.4E-5
HCN	FTIR	-	-	-	-	-	-	-	-	-	-	-	3.7E-5	2.6E-4
C2C*O	GC	-	4.7E-5	3.2E-5	3.7E-5	3.8E-5	8.9E-5	1.1E-4	1.1E-4	9.7E-5	1.1E-4	1.1E-4	1.1E-4	1.2E-4
C2H4	GC	-	-	-	-	-	-	-	-	-	8.3E-6	1.9E-5	3.8E-5	4.0E-5
C2H6	GC	-	-	-	-	-	8.2E-6	8.7E-6	1.1E-5	1.3E-5	2.7E-5	4.6E-5	8.2E-5	1.2E-4
CH3ONO2	GC	-	-	2.3E-5	7.2E-5	8.4E-5	9.3E-5	6.5E-5	-	-	-	-	-	-
ONN(CH3)2	GC	-	-	-	-	-	-	-	-	9.2E-6	2.7E-5	9.0E-5	5.7E-5	6.6E-6
CC*C	GC	-	-	-	-	-	-	-	4.4E-6	3.7E-6	4.3E-6	5.2E-6	1.0E-5	2.8E-5
AceNH2	GC	-	-	-	-	-	1.3E-5	2.1E-5	1.8E-5	1.1E-5	1.1E-5	-	1.1E-5	1.1E-5

The following plots (Figs. S3-S12) show additional comparisons between experimental mole fraction profiles and predictions with the four kinetic models discussed in the main text. The Fuller, Glarborg and Shrestha models mentioned in the captions are slightly modified versions of the original models. These modifications, which have been discussed in detail in the main text, are restricted to the addition of iPN chemistry, which is not part of the original models.

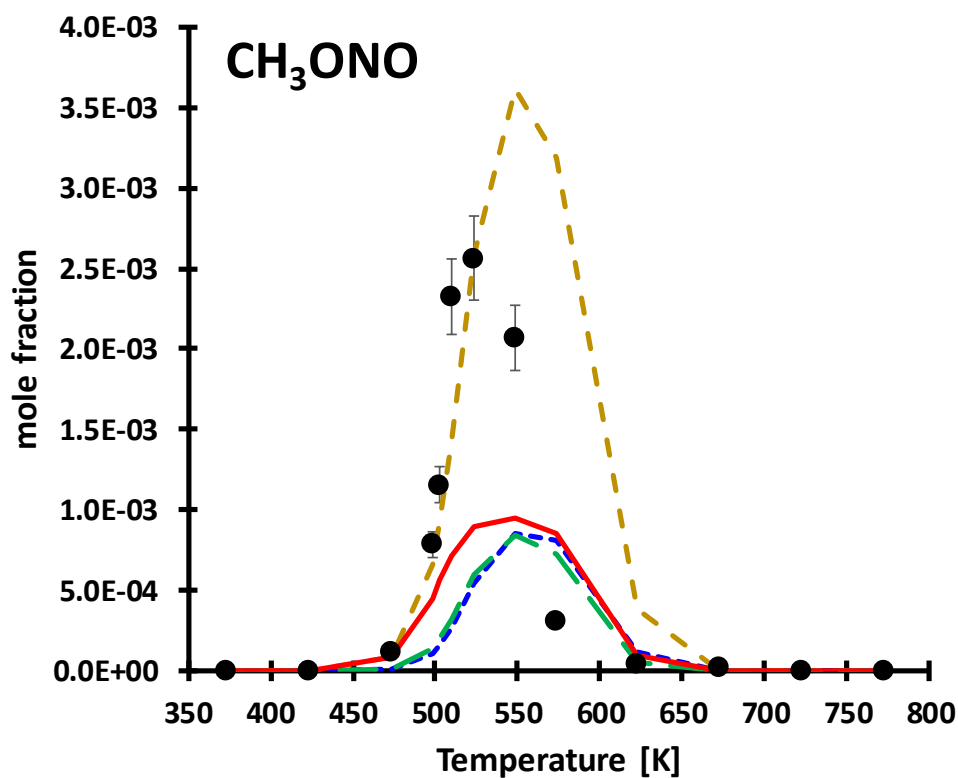


Figure S3: Methyl nitrite mole fractions measured (black filled symbols) in 1% iPN in He pyrolysis. Lines present predictions with the four models discussed in the manuscript: Fuller (solid red), Glarborg (short dashed blue) Shrestha (long dashed green), Mohamed (dashed brown).

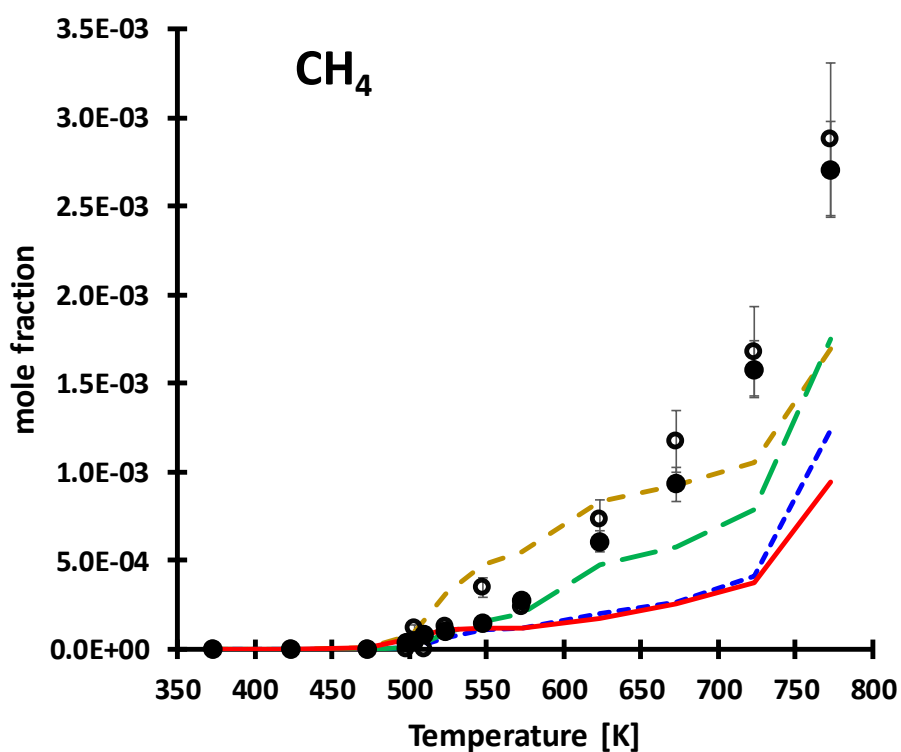


Figure S4: Methane mole fractions measured (black filled symbols) in 1% iPN in He pyrolysis. Lines present predictions with the four models discussed in the manuscript: Fuller (solid red), Glarborg (short dashed blue) Shrestha (long dashed green), Mohamed (dashed brown).

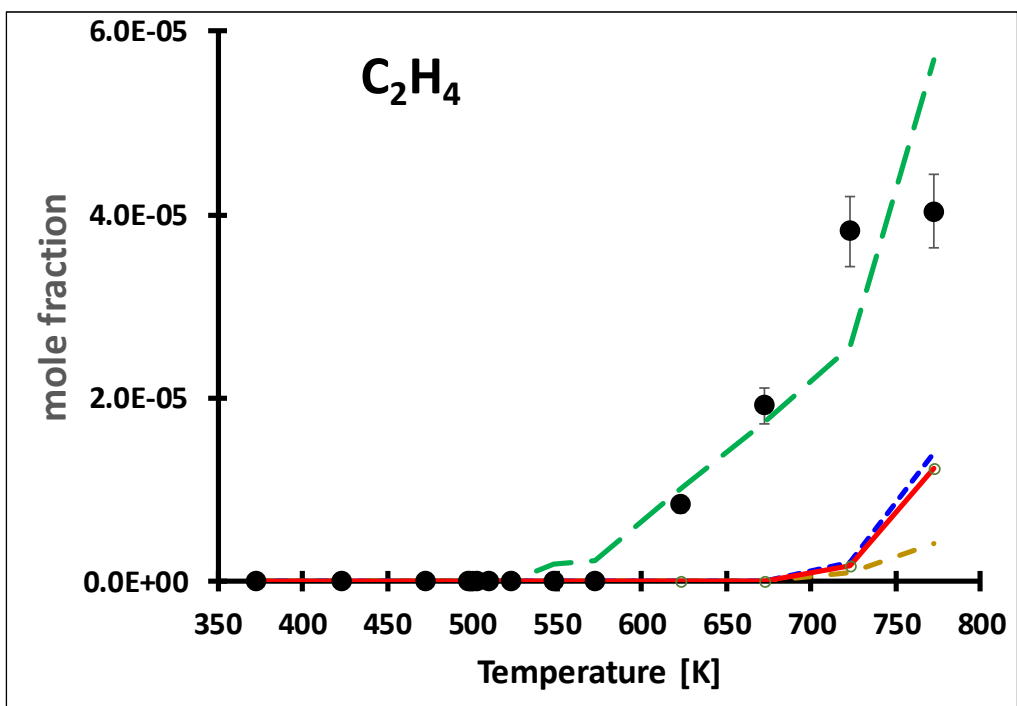


Figure S5: Ethylene mole fractions measured (black filled symbols) in 1% iPN in He pyrolysis. Lines present predictions with the four models discussed in the manuscript: Fuller (solid red), Glarborg (short dashed blue) Shrestha (long dashed green), Mohamed (dashed brown).

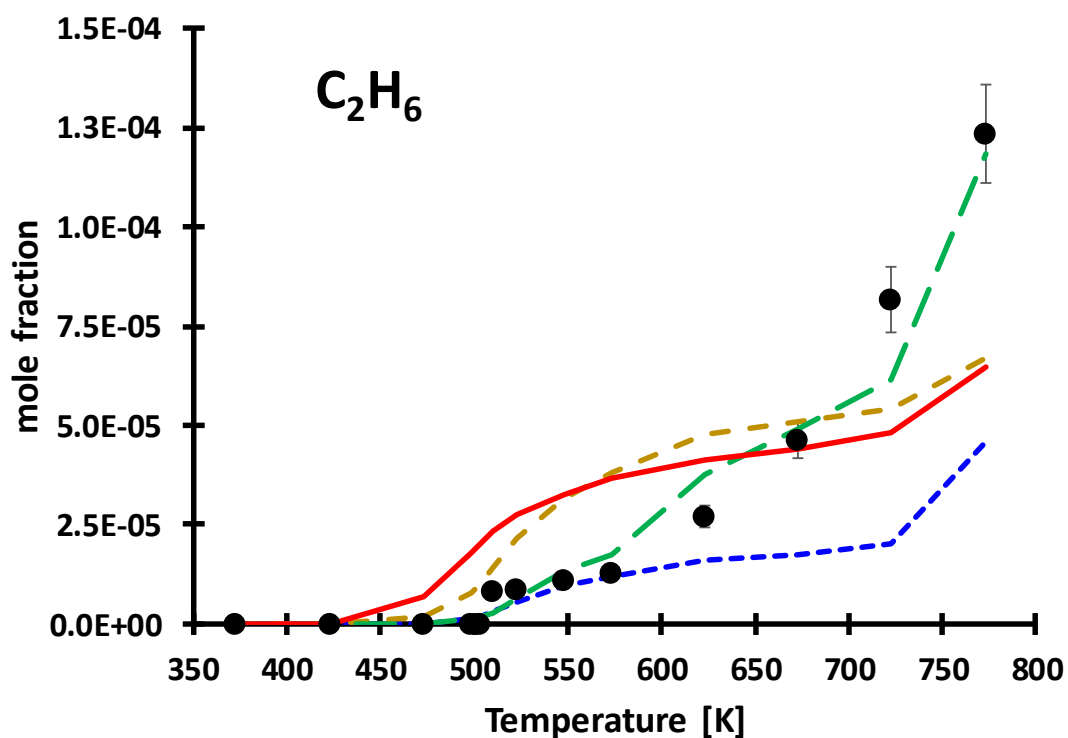


Figure S6: Ethane mole fractions measured (black filled symbols) in 1% iPN in He pyrolysis. Lines present predictions with the four models discussed in the manuscript: Fuller (solid red), Glarborg (short dashed blue) Shrestha (long dashed green), Mohamed (dashed brown).

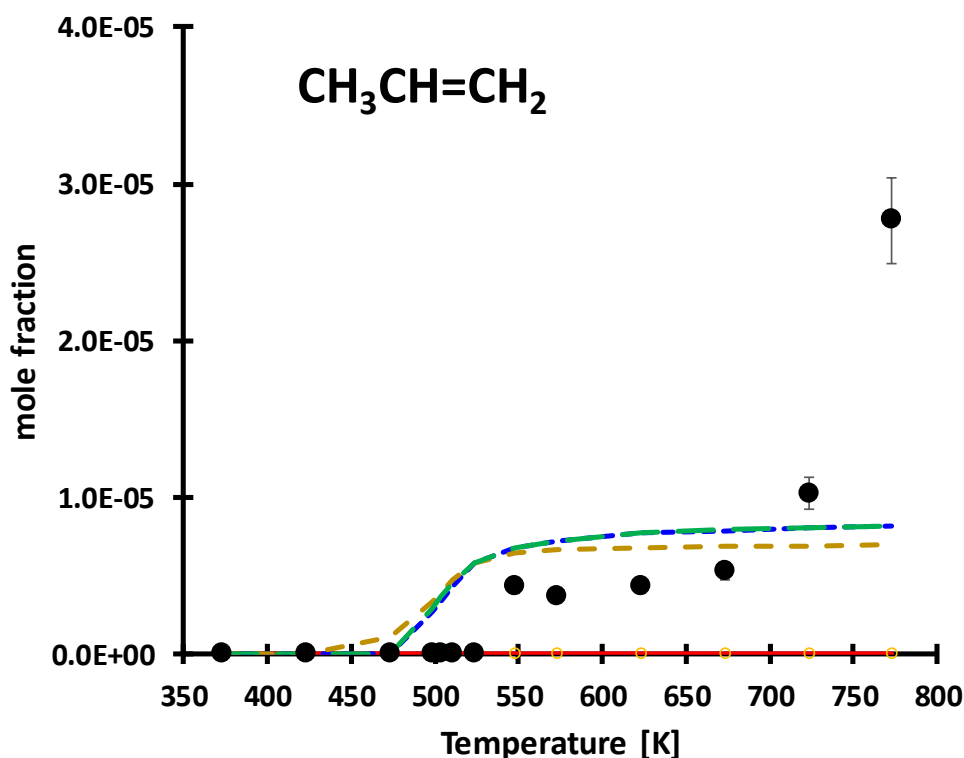


Figure S7: Propene mole fractions measured (black filled symbols) in 1% iPN in He pyrolysis. Lines present predictions with the four models discussed in the manuscript: Fuller (solid red), Glarborg (short dashed blue) Shrestha (long dashed green), Mohamed (dashed brown).

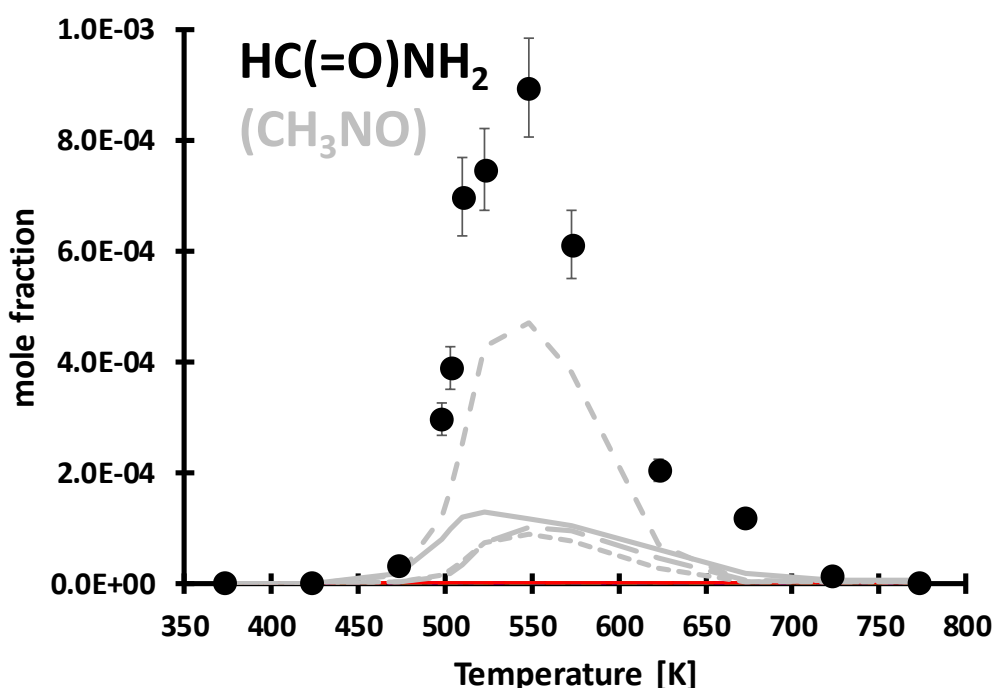


Figure S8: Formamide (HC(=O)NH₂) mole fractions measured (black filled symbols) in 1% iPN in He pyrolysis. Lines present predictions with the four models discussed in the manuscript: Fuller (solid red), Glarborg (short dashed blue) Shrestha (long dashed green), Mohamed (dashed brown). Since none of the models predict formamide to be formed in notable concentrations, this figure also contains the predicted mole fractions for nitrosomethane (CH₃NO), the thermodynamically less stable isomer of formamide. All nitrosomethane profiles are in grey but differ in line type (Fuller: solid; Glarborg: short dashed; Shrestha; long dashed; Mohamed: dashed). The nitrosomethane profile by Mohamed reaches an about four times larger peak value than all other calculated nitrosomethane profiles.

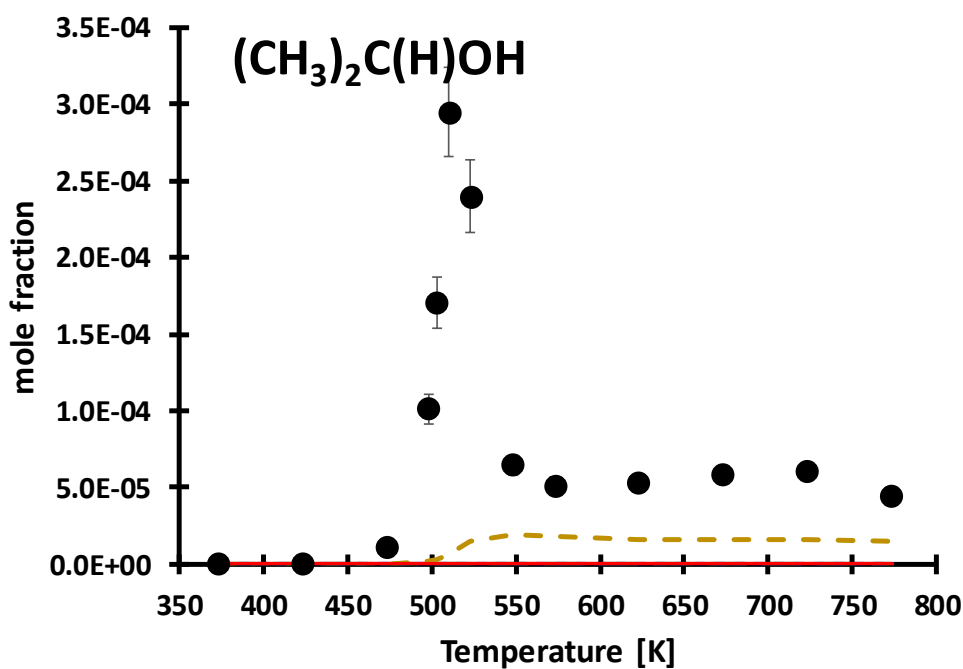


Figure S9: iso-Propanol mole fractions measured (black filled symbols) in 1% iPN in He pyrolysis. Lines present predictions with the four models discussed in the manuscript: Fuller (solid red), Glarborg (short dashed blue) Shrestha (long dashed green), Mohamed (dashed brown).

The narrow peak around 500 K strongly suggests that iso-propanol formation is correlated with the presence of iPN.

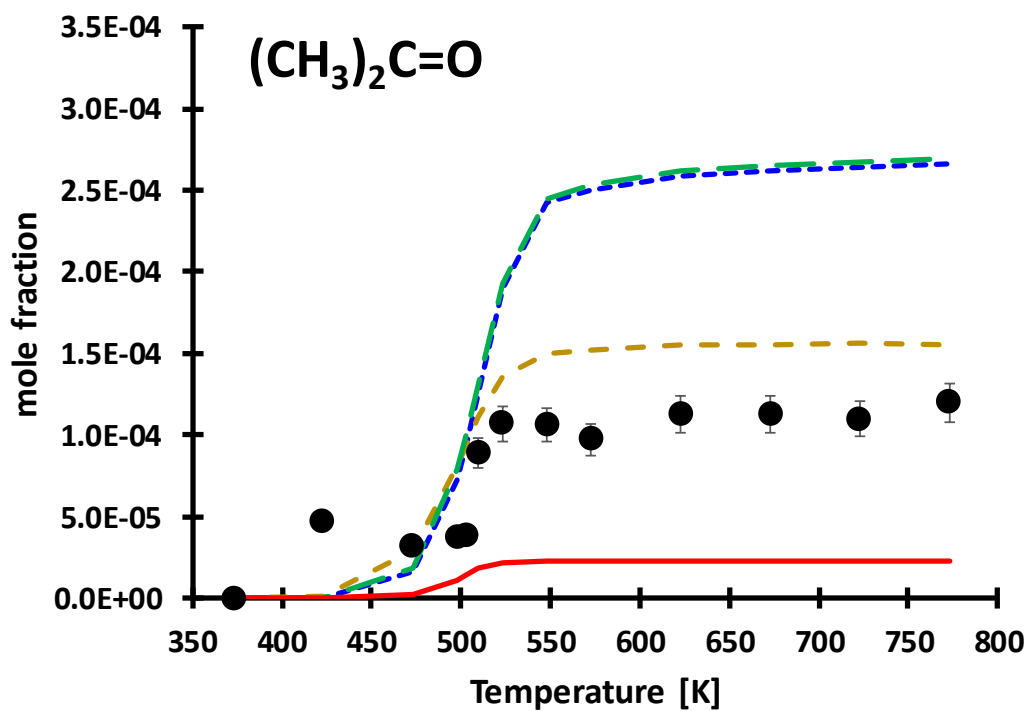


Figure S10: Acetone mole fractions measured (black filled symbols) in 1% iPN in He pyrolysis. Lines present predictions with the four models discussed in the manuscript: Fuller (solid red), Glarborg (short dashed blue) Shrestha (long dashed green), Mohamed (dashed brown).

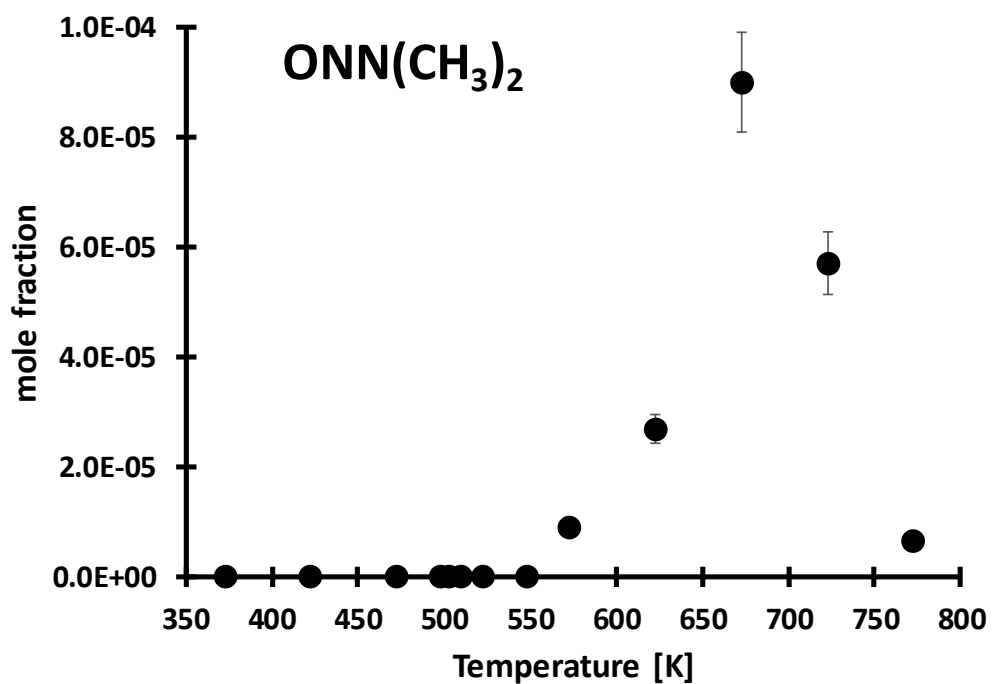


Figure S11: Dimethylnitrosoamine mole fractions measured (black filled symbols) in 1% iPN in He pyrolysis. None of the four models used in this study predicts mole fractions for this species.

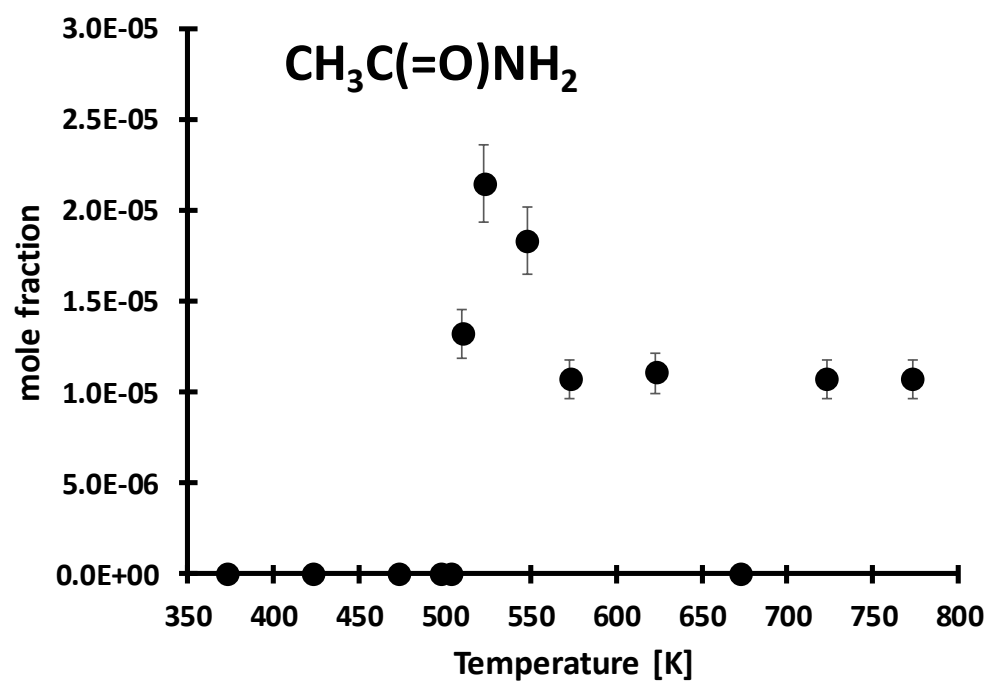


Figure S12: Acetamide mole fractions measured (black filled symbols) in 1% iPN in He pyrolysis. None of the four models used in this study predicts notable mole fractions for this species.

6. Pressure-dependent rate coefficients for iPN decomposition

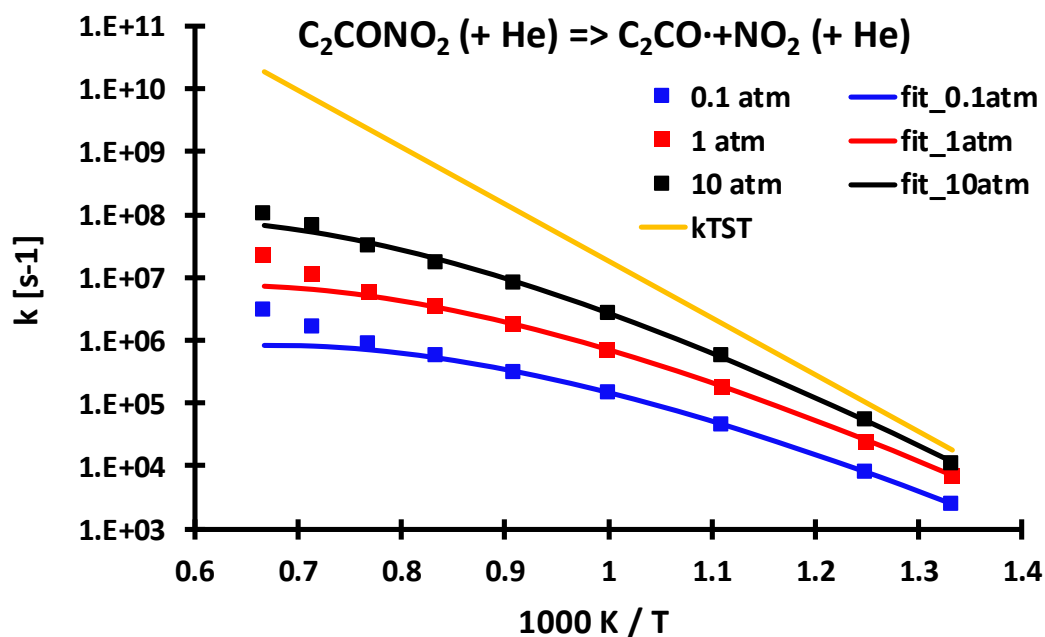


Figure S13: Pressure-dependent rate coefficients for iPN (C₂CONO₂) decomposition in helium (He) and comparison with the high-pressure (TST) rate expression. The modified Arrhenius expressions shown as solid lines are obtained from fits using only the rate coefficients up to 1100 K because at higher temperatures contributions from direct (non-thermal) contributions become important as the positive deviations between data points and lines show. The pressure-dependent analysis was done with MultiWell software^{1,2}. Other product channels contribute to less than 0.1 % at any conditions investigated.

7. Ab initio energies related to iPN and CH₃NO₂

Table S5: Comparison between relative energies for the iPN PES calculated at various ab initio levels with Fuller et al.³. All values are for 0K and in kcal/mol.

Species	CBS-QB4 (0K)	G4 (0K)	CCSD(T)/CBS			Fuller et al. ³
			cc-pV(D/T)Z	cc-pV(T/Q)Z	aug-cc-pV(D/T)Z	
iPN	0	0	0	0	0	0
C2COJ+NO2	43.8	41.3	42.8	42.7	42.9	41.9 (40.9 [*])
TS: iPN → C2C=O+HONO	41.4	41.2	42.7	42.0	42.0	42.6
C2C=O+HONO	-23.6	-24.7	-24.9	-25.6	-24.8	-25.5
TS: iPN → C=CC+HONO2	44.0	43.2	44.4	42.7	43.6	N/A
C=CC+HONO2	19.8	18.6	18.1	18.1	19.0	N/A

* optimized value for improved agreement with experiments

The G4 values are generally relatively close to the best CCSD(T)/CBS value, which is the one that uses T/Q basis sets. Rather large deviations between the various CCSD(T)/CBS extrapolations suggests that higher levels of theory are needed. Those are not affordable with the computational resources available to the authors.

Table S6: Comparison between relative energies for the CH₃NO₂ reaction system calculated at various ab initio levels with the ATcT recommended values and with results from Annesley et al. The enthalpies are for 0 K and 298 K (in parenthesis) and given in kcal/mol.

Species	G4 0K (298 K)	CCSD(T)/CBS				ATcT 1.122r ₄	Annesley ^{*5}
		cc-pV(D/T)Z	cc-pV(T/Q)Z	aug-cc-pV(D/T)Z	aug-cc-pV(T/Q)Z		
CH ₃ NO ₂	0	0	0	0	0	0	
c-CH ₃ ONO	2.3 (2.7)	1.0	2.0	1.1	1.8	1.3 (1.8)	
CH ₃ +NO ₂	58.6 (60.5)	58.8	59.9	59.4	59.7	59.2 (61.0)	
CH ₂ O+HNO	16.6 (18.3)	15.1	15.5	15.6	15.4	15.6 (17.3)	
CH ₃ O+NO	42.9 (44.4)	41.9	43.2	42.5	43.2	43.1 (44.8)	

* CCSD(T)/CBS//CASPT2 aug-cc-pVTZ (atz) results using aug'-cc-pVQZ (a'qz) and aug'-cc-pV5Z (a'5z) basis sets for the extrapolation

The Annesley values are in full agreement with the ATcT values (accessed August 2022), suggesting that their kinetic analysis of the CH₃NO₂ system is highly accurate. The G4 values are within 1 kcal/mol of the ATcT results.

8. PES of C₂JCONO₂

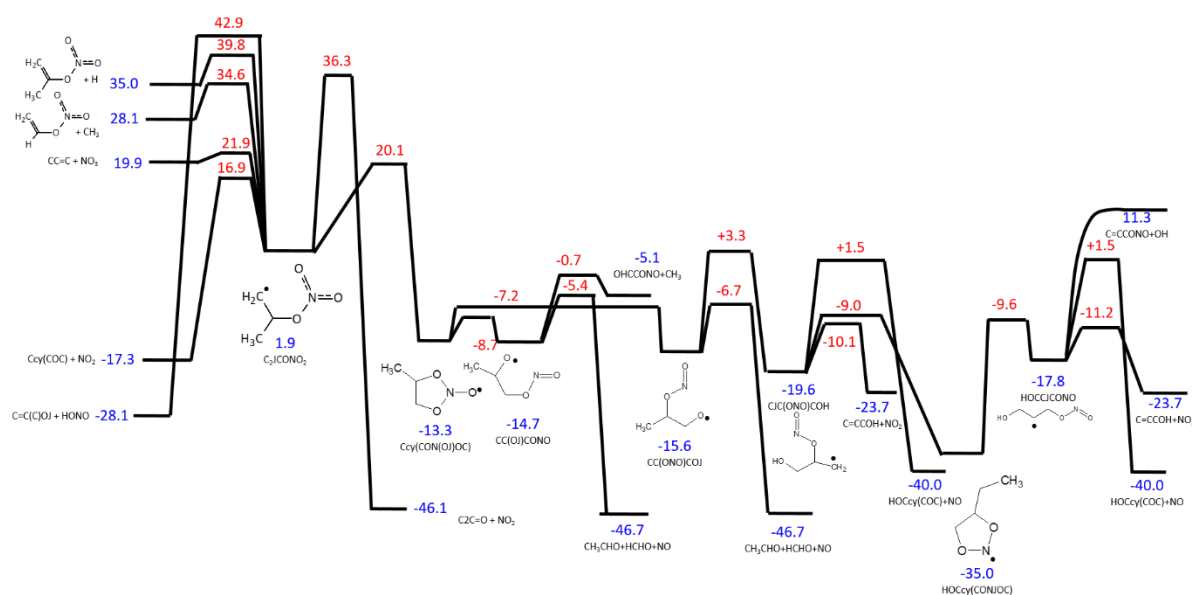


Figure S14: CBS-QB3 calculated potential energy surface (enthalpies of formation at 298 K) for the iPN radical $\text{CH}_3\text{C(H)(ONO}_2\text{)CH}_2$, labelled C_2JCONO_2

All data shown in Figure S14 are taken from CBS-QB3 calculations, however the barriers for the initial reactions of C_2JCONO_2 have also been calculated at the G4 level of theory. The G4 results for the three lowest energy channels were used to create the input files for the MultiWell analysis.

Table S7: Comparison of the relative barrier heights for the first three transition states using CBS-QB3 and G4 methodology. All energies in kcal/mol are relative to the initial well C_2JCONO_2 .

TS	CBS-QB3 (0K)	G4 (0K)	CCSD(T)/CBS	
			cc-pV(D/T)Z	aug-cc-pV(D/T)Z
$\text{C}_2\text{JCONO}_2 \rightarrow \text{CC}=\text{C}+\text{NO}_3$	19.8	20.3	21.2	20.5
$\text{C}_2\text{JCONO}_2 \rightarrow \text{Ccy}(\text{COC})+\text{NO}_2$	15.3	19.0	19.6	18.6
$\text{C}_2\text{JCONO}_2 \rightarrow \text{Ccy}(\text{CON(O)OC})$	19.2	20.3	21.5	21.1

The CCSD(T)/CBS extrapolated relative energies are in relative good agreement with the G4 values and higher than the CBS-QB4 barriers. Only for the ring-forming reaction, the difference between CCSD(T)/CBS and G4 is above 1 kcal/mol. Due to the tight transition state, this reaction does not play an important role even if the barrier is as low as G4 predicts. The transition states of other reaction channels are at least 10 kcal/mol higher than those included in Table S7 and do not play any role at the experimental conditions.

9. Pressure-dependent rate expressions for unimolecular decomposition of the iPN radical $\text{CH}_3\text{C}(\text{H})(\text{ONO}_2)\text{CH}_2$, labelled C_2JCONO_2

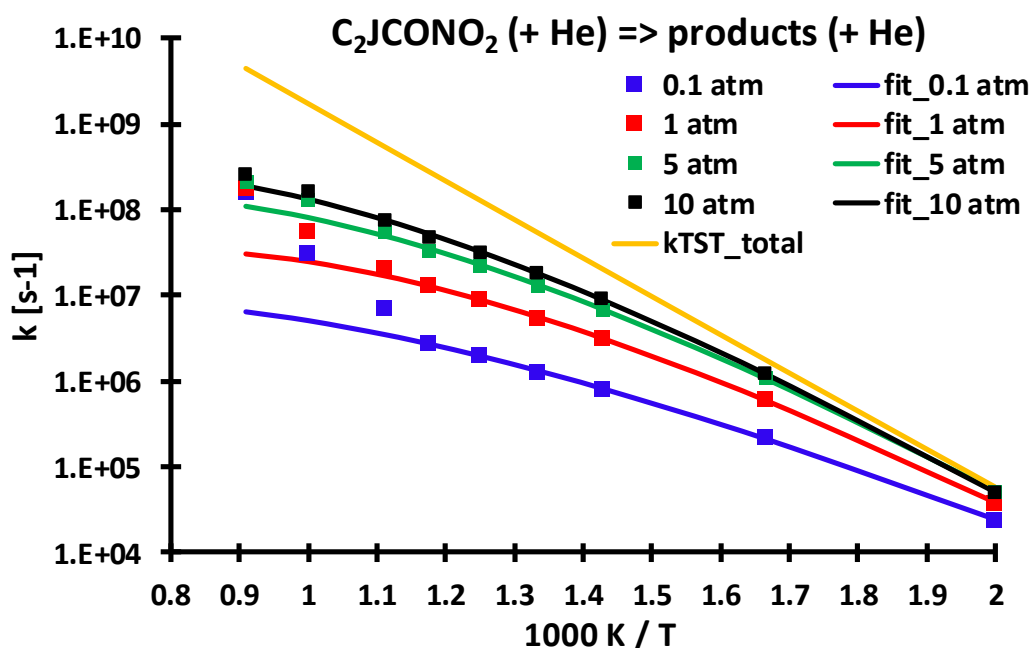


Figure S15: Pressure-dependent rate coefficients for iPN radical (C_2JCONO_2) decomposition in helium (He) and comparison with the high-pressure (TST) rate expression. The modified Arrhenius expressions shown as solid lines are obtained from fits using only the rate coefficients up to 850 K because at higher temperatures contributions from direct (non-thermal) contributions become important as the positive deviations between data points and lines show. The pressure-dependent analysis was done with MultiWell software^{1,2}.

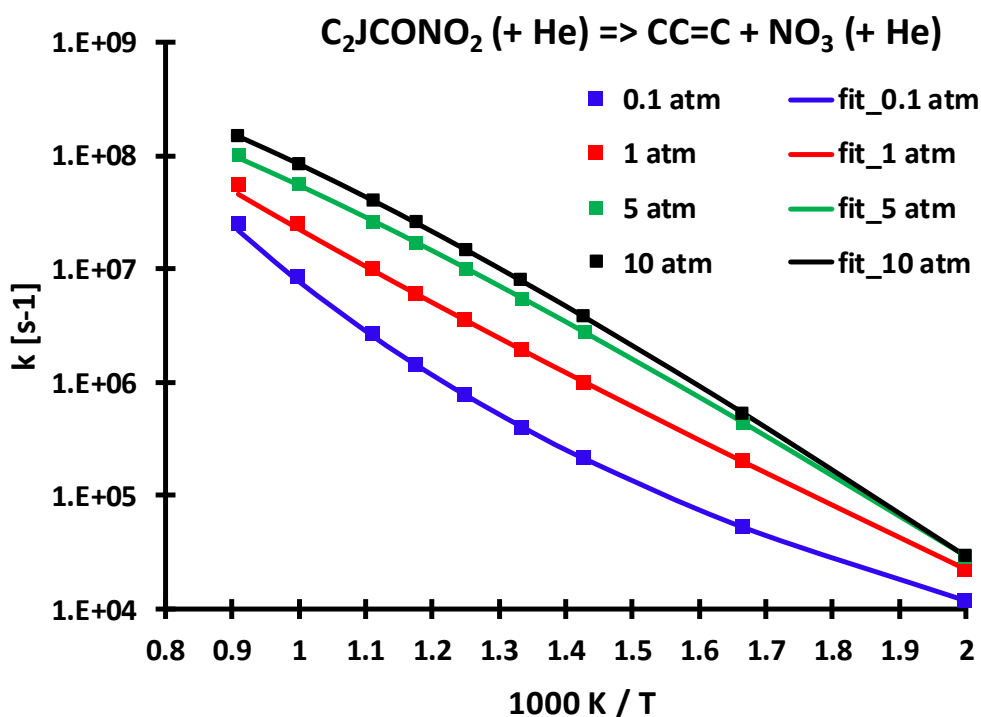


Figure S16: Pressure-dependent rate coefficients for the iPN radical (C_2JCONO_2) decomposition channel to propene and nitrogen trioxide in helium (He). The modified Arrhenius expressions shown as solid lines are from fits using only the rate coefficients up to 850 K but they reproduce the data over the entire temperature range (500 K – 1100 K) well.

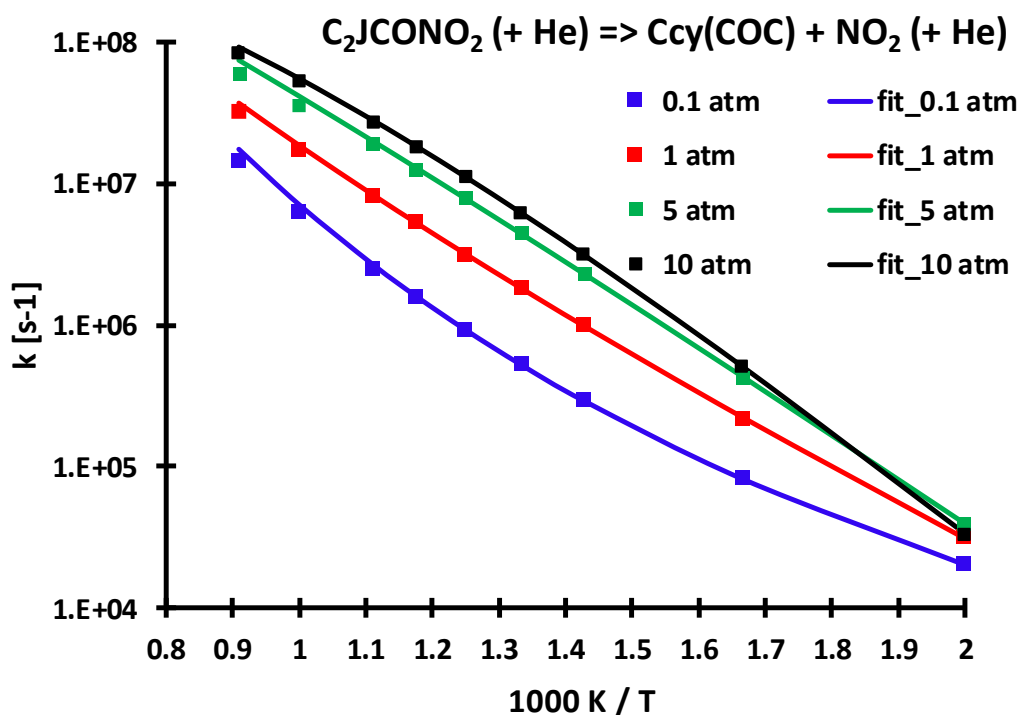


Figure S17: Pressure-dependent rate coefficients for the iPN radical (C_2JCONO_2) decomposition channel to methyloxirane and nitrogen dioxide in helium (He). The modified Arrhenius expressions shown as solid lines are from fits using only the rate coefficients up to 850 K. They reproduce the data over the entire temperature range (500 K – 1100 K) well.

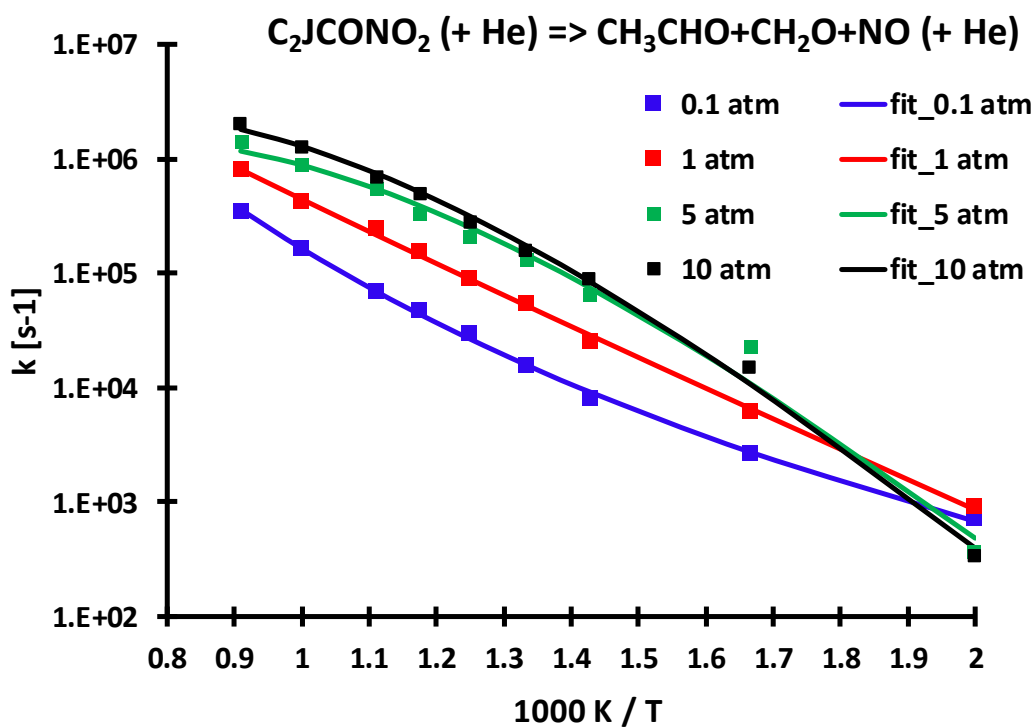


Figure S18: Pressure-dependent rate coefficients for the iPN radical (C_2JCONO_2) decomposition channel to acetaldehyde, formaldehyde and methyloxirane and nitrogen monoxide in helium (He). All data were used for the fits because this is a minor channel and the data at low temperature contain a large statistical error due to small sample sizes.

10. High-pressure limit rate coefficients for $\text{CH}_3\text{NO}_2 \rightarrow \text{CH}_3 + \text{NO}_2$

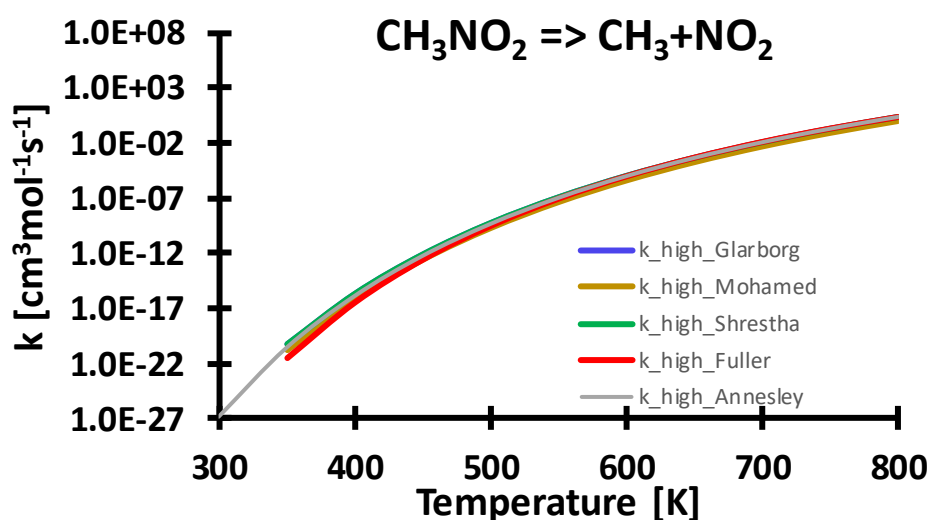


Figure S19: High-pressure rate coefficients used by the four kinetic models employed in this study. Fuller et al. ^{3,6} red; Shrestha et al. ⁷ green; Glarborg et al. ⁸ blue; Mohamed et al. ⁹ brown, Also included is the high-pressure rate expression reported by Annesley et al. ⁵ (grey line).

The main point of Figure S19 is to show the large uncertainty of this rate expressions (note the huge scale of the y-axis) at low temperatures. Since all kinetic models tested in this study use this rate expression to calculate the kinetic coefficient for the “reverse” reaction $\text{CH}_3 + \text{NO}_2 + \text{M} \rightarrow \text{CH}_3\text{NO}_2 + \text{M}$, these uncertainties have a significant impact on the predictions. “Reverse” is placed in quotes because strictly these two reactions are not forward and reverse reactions because $\text{CH}_3 + \text{NO}_2 + \text{M} \rightarrow \text{CH}_3\text{NO}_2 + \text{M}$ is a chemically activated reaction, which leads to a different state population in $[\text{CH}_3\text{NO}_2]^*$, the chemically activated complex, than found in the collisionally activated dissociation of CH_3NO_2 . This being said, an improved way to implement the reaction $\text{CH}_3 + \text{NO}_2 + \text{M} \rightarrow \text{CH}_3\text{NO}_2 + \text{M}$ would be to include it as an irreversible reaction and to assign its pressure-dependent rate expression from the solution of the appropriate Master Equation (ME), e.g. using MultiWell as solver. Since the high-pressure rate coefficient is needed as input for such an analysis, a very brief review about the current knowledge of the $\text{CH}_3 + \text{NO}_2$ reaction is given next.

11. Brief review of the High-pressure limit rate coefficients for the reactions $\text{CH}_3+\text{NO}_2 \rightarrow \text{CH}_3\text{O}+\text{NO}$ and $\text{CH}_3+\text{NO}_2 \rightarrow \text{CH}_3\text{NO}_2$

In 1974 Glänzer and Troe¹⁰ studied both reaction channels



and



at the same conditions. The results are shown as red lines in Figure S20.

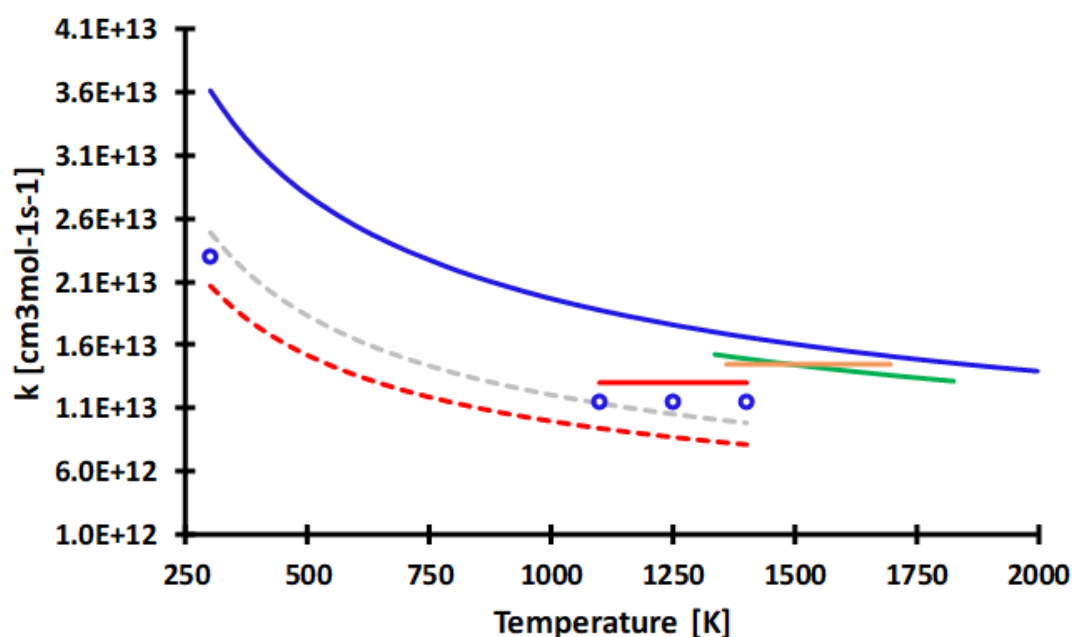


Figure S20: Selected high-pressure rate expressions for the CH_3+NO_2 addition reactions. Solid lines: CH_3ONO channel; Annesley⁵ (blue), Matsugi¹¹ (green), Glänzer¹⁰ (red), Srinivasan¹². Broken lines: CH_3NO_2 channel; Glänzer¹⁰ (dashed red), Annesley⁵ (open blue circles), representative curve of Annesley data (dashed grey).

For the $\text{CH}_3\text{O}+\text{NO}$ channel (Rxn 3) only high-temperature data were measured which suggest that the reaction rate coefficient is temperature independent. Newer data by Annesley⁵ suggest a negative temperature dependence for the rate coefficient for Rxn 3. In this recent study, Annesley et al.⁵ provide high-level electronic structure calculations describing the potential energy surfaces for the dissociation of nitromethane and methyl nitrite. Although mainly used to address the question of the importance of roaming in nitromethane dissociation, the authors also briefly report on high-pressure limit rate coefficients for the two CH_3+NO_2 association reactions. At room temperature the rate coefficient for Rxn 4 is $3.8 \times 10^{-11} \text{ cm}^3 \text{ molecule}^{-1} \text{ s}^{-1}$ ($2.3 \times 10^{13} \text{ cm}^3 \text{ mol}^{-1} \text{ s}^{-1}$) while for Rxn 3, a value of $5.9 \times 10^{-11} \text{ cm}^3 \text{ molecule}^{-1} \text{ s}^{-1}$ ($3.6 \times 10^{13} \text{ cm}^3 \text{ mol}^{-1} \text{ s}^{-1}$) can be extracted from Figure 10 of that work. Annesley et al. note that their result for the $\text{CH}_3\text{O}+\text{NO}$ channel is more than a factor of two larger than the value used in the literature at that time (e.g. the Glänzer and Troe data), which is beyond the expected uncertainty of their calculation. One year later, Matsugi et al.¹¹ reported new experimental values for this reaction supporting a higher rate coefficient for Rxn 3. This new data agrees rather well with the predictions by Annesley et al. (Figure S20). Since Annesley et al. did not provide a rate expression for Rxn 4, such an expression is estimated in Figure S20, by scaling the expression provided

by Glänser and Troe by 1.1 to roughly match the results mentioned by Annesley. This rate expression has been used in the current study as input for the Multiwell master equation analysis to evaluate the pressure-dependence of Rxn 4 with helium as bath gas. Figure 7 of the main text shows the results and one can notice that at 550 K and 1 atm the rate coefficient is only about $\frac{1}{4}$ of the high-pressure limit.

12. References

- (1) Barker, J. R.; Nguyen, T. L.; Stanton, J. F.; Aieta, C.; Ceotto, M.; Gabas, F.; Kumar, T. J. D.; Li, C. G. L.; Lohr, L. L.; Maranzana, A.; et al.: University of Michigan, Ann Arbor, Michigan, USA, 2017.
- (2) Barker, J. R. *International Journal of Chemical Kinetics* **2001**, *33*, 232.
- (3) Fuller, M. E.; Goldsmith, C. F. *The Journal of Physical Chemistry A* **2019**, *123*, 5866
- (4) Ruscic, B.; Pinzon, R. E.; von Laszewski, G.; Kodeboyina, D.; Burcat, A.; Leahy, D.; Montoya, D.; Wagner, A. F. *Journal of Physics: Conference Series SciDAC 2005* **2005**, *16*, 561
- (5) Annesley, C. J.; Randazzo, J. B.; Klippenstein, S. J.; Harding, L. B.; Jasper, A. W.; Georgievskii, Y.; Ruscic, B.; Tranter, R. S. *The Journal of Physical Chemistry A* **2015**, *119*, 7872
- (6) Fuller, M. E.; Mousse-Rayaleh, A.; Chaumeix, N.; Goldsmith, C. F. *Combustion and Flame* **2022**, *242*, 112187.
- (7) Shrestha, K. P.; Vin, N.; Herbinet, O.; Seidel, L.; Battin-Leclerc, F.; Zeuch, T.; Mauss, F. *Fuel* **2020**, *261*, 116349.
- (8) Glarborg, P.; Miller, J. A.; Ruscic, B.; Klippenstein, S. J. *Progress in Energy and Combustion Science* **2018**, *67*, 31
- (9) Mohamed, A. A. E.-S.; Panigrahy, S.; Sahu, A. B.; Bourque, G.; Curran, H. *Combustion and Flame* **2022**, *241*, 112058.
- (10) Glänzer, K.; Troe, J. *Berichte der Bunsengesellschaft für Physikalische Chemie* **1974**, *78*, 182
- (11) Matsugi, A.; Shiina, H. *The Journal of Physical Chemistry A* **2017**, *121*, 4218
- (12) Srinivasan, N. K.; Su, M.-C.; Sutherland, J. W.; Michael, J. V. *The Journal of Physical Chemistry A* **2005**, *109*, 1857